Preparation and characterization of poly(o-toluidine)/ nano TiO_2 composite and study of their anticorrosion properties blended with epoxy resin

CHUANBO HU[A,B], JIAWEI LI[A,B], YAZHOU KONG[A,B], YUSHI DING[A,B] AND YING LI[A,B]*

[a] *School of Metallurgy, Northeastern University, Shenyang 110819, China*
[b] *Liaoning Key Laboratory for Metallurgical Sensor and Technology, Northeastern University, Shenyang 110819, China*

ABSTRACT

In this investigation, HCl doped poly(o-toluidine)/nano TiO_2 composite was prepared using in situ polymerization method. The composition and structure of the composite were characterized by Fourier transformation infrared spectroscopy (FT-IR), UV-visible spectroscopy (UV-vis), X-ray diffraction (XRD), Scanning electron microscopy (SEM) and Thermogravimetric analysis (TGA). The anticorrosion properties of the epoxy resin blended with poly(o-toluidine)/ nano TiO_2 composite were studied in 3.5% NaCl solution by electrochemical measurements. Potentiodynamic polarization measurement showed that poly(o-toluidine)/nano TiO_2/epoxy composite coating acted as a highly efficient corrosion protection layer on steel with 97.85% protection efficiency. Electrochemical impendence spectroscopy measurement showed that poly(o-toluidine)/nano TiO_2/epoxy composite coating exhibited a higher charge transfer resistance and effectively decreased the permeation of water and corrosion substances. The highly efficient corrosion protection of the epoxy coating containing poly(o-toluidine)/nano TiO_2 composite may be derived from the passivation and barrier effects.

KEY WORDS : *Poly(o-toluidine)/nano TiO_2 composite, Anticorrosion properties, Passivation, Barrier*

1. INTRODUCTION

Polyaniline (PANI) derivatives have received much attention because of its superior solubility and processibility, excellent thermal stability and anticorrosion property [1–3]. The previous studies [4–6] revealed that the introduction of the alkyl or alkoxy groups on the benzene ring could significantly improve the anticorrosion property of PANI and the solubility in a conventional solvent, which may due to the steric hindrance and π-electron effects of

J. Polym. Mater. Vol. **34,** No. 4, 2017, 797-808

Correspondence author e-mail:liying@mail.neu.edu.cn

substituted PANI [7,8]. Besides, the larger molecular size of PANI derivatives facilitates a greater coverage surface and leads to a better adhesion to the metal substrates [9]. Ma et al. [10] prepared the soluble phosphoric acid doped poly(2,3-dimethylaniline) (P(2,3-DMA)) by chemical polymerization method. The corrosion analysis showed that the anticorrosion property of the uniform and strongly adherent P(2,3-DMA) coating was better than PANI, owing to its relatively good solubility and the electronic-donating substitution effects.

Furthermore, the literatures [11–13] reported that PANI/inorganic composite would improve the thermal stability, mechanical properties, anticorrosion properties and adhesion to the substrate as well. Mostafaei et al. [14] observed that epoxy/PANI/ZnO composite coated steel exhibited higher anticorrosion properties and provided better barrier properties than that of epoxy/PANI composite coated steel in 3.5% NaCl solution. O-toluidine (OT) is one kind of the derivatives of aniline. It has been used as dyes, pesticides, pharmaceuticals and organic intermediates. The methyl on the ortho position of the amino group could lead to high steric hindrance between the molecular chains. Therefore, the rigid molecular chains of PANI can be effectively decreased and the solubility of PANI can be improved. Titanium dioxide (TiO_2) has received great attention because of its unique optical and electrical properties such as charge carrier, oxidizing power, nontoxic properties, chemical and photo stability. Specifically, titanium dioxide has been widely used in heterogeneous catalysis, photocatalyst, in solar cell for the production of hydrogen, electric energy, gas sensor, white pigment, anticorrosion coatings and electrochromic devices [15]. In this study, poly(o-toluidine)/nano TiO_2 composite was prepared by in situ polymerization method in hydrochloric acid medium, and was used to prepared poly(o-toluidine)/nano TiO_2/epoxy composite coating. The composite coating containing poly(o-toluidine)/nano TiO_2 composite inclusion was characterized by FT-IR, UV-vis, XRD, SEM and TGA. The anticorrosion properties of poly(o-toluidine)/nano TiO_2/epoxy composite coated steel were investigated by potentiodynamic polarization and electrochemical impedance spectroscopy in 3.5% NaCl solution as corrosion environment, and also compared with that of poly(o-toluidine)/epoxy composite coated steel.

2. EXPERIMENTAL

2.1 Materials

All chemical reagents used in this study were of analytical laboratory grade, and were purchased from different sources. O-toluidine (OT) monomer was distilled to colorless before use, and all the other chemical reagents used were without any further purification. Butyl alcohol and N-methyl-2-pyrrolidone (NMP) were purchased from Tianjin Kemiou Chemical Reagent Co., Ltd. Hydrochloric acid (HCl), sodium chloride (NaCl), ammonium persulfate (APS) and dibutyl phthalate were purchased from XiLong Chemical Co., Ltd. OT, ethanol and ethyl acetate were purchased from KeLong Chemical Reagent Co., Ltd. Epoxy resin (EP) and polyamide were purchased from Yichun Yuanda Chemical Co., Ltd. TiO_2 nanoparticles with particle size of 10 nm were obtained from Shanghai River Industrial Co., Ltd.

2.2. Preparation of poly(o-toluidine)/nano TiO_2 composite

Poly(o-toluidine)/nano TiO_2 composite (PTC) was prepared by in situ polymerization. 10.67 mL OT monomer was added to 100 mL 1.0 M HCl solution, and then 0.80 g TiO_2 nanoparticles were added to the clear

solution with magnetic stirring for 30 min to reduce the aggregation of TiO_2 nanoparticles. After that, 22.82 g APS was dissolved in a 150 ml 1.0 M HCl solution and the solution was added dropwise to the above solution under vigorous stirring in an ice bath. The polymerization process was continuously stirred for 10 h to ensure complete polymerization. The products were filtered and washed with ethanol and deionized water until the filtrate turned colorless. Finally, the filter cake was dried in air oven at 60 °C for 20 h. In the same method, pure POT was also prepared without TiO_2 nanoparticles for comparing the structure and anticorrosion properties with PTC.

2.3. Characterization

The FT-IR spectra of the samples were recorded using a Nicolet 380 spectrometer by the KBr pellet technique in the range of 4000~500 cm^{-1}. The UV-vis spectra of the samples were recorded using a UV-2102PC spectrophotometer in the range of 200~850 nm, the samples were prepared by dissolving a small amount of powder in NMP solvent. The XRD patterns of the samples were recorded using a DX-2700 X-ray diffraction in the range of 10°~90°. The TGA curves of the samples were performed using a STA-449C thermal analyzer in air from 25 °C to 800 °C at the heating rate of 10 °C/min. The morphological structures of the samples were observed using a S-3400N digital scanning electron microscopy.

2.4. Preparation of the composite coatings

The steel samples were cut into 2 cm×2 cm dimension and the surface were polished using 320, 600 and 1000 grade emery papers respectively, followed by degreasing with acetone and ethanol solvents, and then airdried at room temperature before coated. PTC or POT powders as the fillers were dispersed in epoxy and polyamide system by ultrasound, the quantity of the fillers was 5 % out of the quantity of epoxy resin (the quantity of epoxy was 2.5 g). The butyl alcohol and NMP mixture was used as the solvent, dibutyl phthalate was used as the plasticizer and ethyl acetate was used as the defoaming agent. The steel samples were coated with the composite coatings and cured for 24 h at room temperature after being cured for 12 h at 60 °C. Uncoated steel was used as reference sample to compare the anticorrosion properties with pure epoxy (EP) coated steel, POT/epoxy (POT/EP) composite coated steel and PTC/epoxy (PTC/EP) composite coated steel. The thickness of the composite coating was 100±5 μm. Figure 1 shows the schematic preparation of HCl doped poly(o-toluidine)/nano TiO_2/epoxy composite coating onto the steel surface.

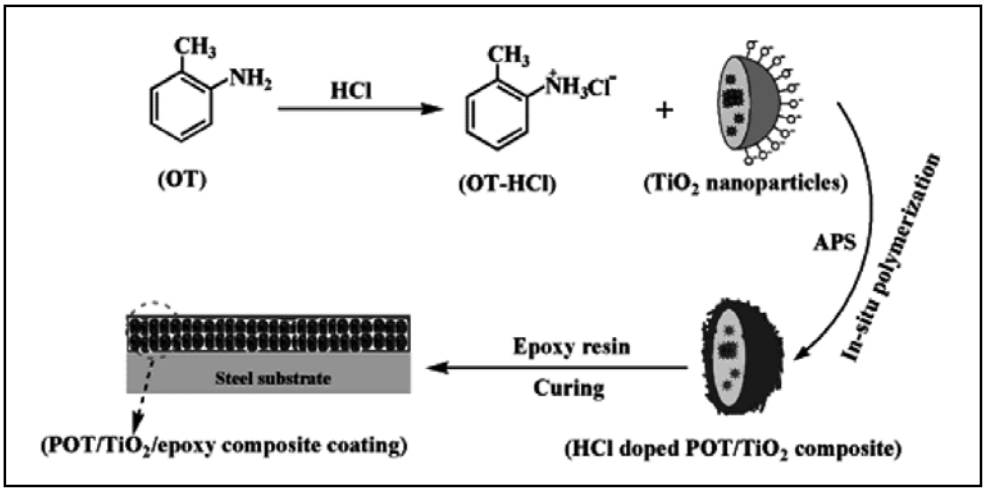

Fig. 1. The schematic preparation of HCl doped poly(o-toluidine)/nano TiO_2/epoxy composite coating onto the steel surface.

2.5. Electrochemical corrosion studies

The anticorrosion properties of the uncoated and coated steel samples were measured by the electrochemical corrosion methods. The data were tested in 3.5% NaCl solution using a CHI660D electrochemical workstation. The potentiodynamic polarization and electrochemical impedance spectroscopy (EIS) were recorded using a three-electrode electrochemical cell with saturated calomel electrode (SCE) as reference electrode, and platinum gauze as counter electrode and the uncoated and coated steel samples were used as working electrodes. The potentiodynamic polarization was measured between –1.2~0.2 V (vs. SCE) at a scan rate of 5 mV/s, the corrosion data were obtained through superimposing a straight line along the linear portion of the cathodic and anodic curves. The EIS was measured at the frequency range of 100 kHz~10 mHz with an AC amplitude of 10 mV.

3. RESULTS & DISCUSSIONS

3.1. FT-IR analysis

Figure 2 shows the FT-IR spectra of TiO_2, POT and PTC, Table 1 shows the characteristic absorption peaks of POT and PTC. As shown in Fig. 2 and Tab. 1, the spectra appearance and wavenumber of POT and PTC are consistent with the literatures reported [16,17]. Compared to the wavenumber of POT, it can be seen that the characteristic peaks of PTC have shifted to lower wavenumbers, which indicates a certain physicochemical interaction existed between POT and TiO_2 nanoparticles. The certain physicochemical interaction may be the hydrogen bond [18], which generates from interaction between the hydroxyl on the surface of TiO_2 and the imines of POT. In the case of TiO_2 nanoparticles the strong absorption peak

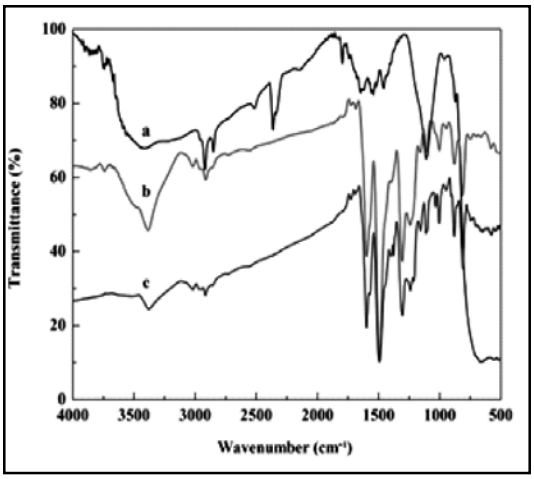

Fig. 2. FT-IR spectra of (a) TiO_2, (b) POT and (c) PTC.

TABLE 1 The FT-IR spectra wavenumber data of POT and PTC.

Characteristic peaks	Wavenumber (cm^{-1})	
	POT	PTC
N-H stretching	3390	3385
C-H methyl stretching	2913	2908
C=C quiniod stretching	1596	1592
C=C benzenoid stretching	1494	1487
C-N stretching	1307	1302
C–H plane stretching	1162	1158
C-H out plane bending	817	815

centred at around 670 cm^{-1} due to Ti-O stretching [19] is observed, while this peak is found to be weak in PTC due to the presence of POT. These results suggests that TiO_2 nanoparticles are effectively covered by POT.

3.2. UV-vis analysis

Figure 3 shows the UV-vis spectra of POT and PTC. From Fig. 3a, it can be observed that POT has two characteristic peaks at around 313 and 619 nm. The peak at around 313 nm is assigned to π–π^* transition of the benzenoid rings, while the peak at around 619 nm is attributed to n–π^* transition of benzenoid to quinoid rings [20,21]. As shown in Fig. 3b, the UV-vis spectra shapes of PTC are similar to POT and the characteristic peaks are slight blue shifted to 311 and 612 nm respectively, and the intensity of absorption peaks increase.

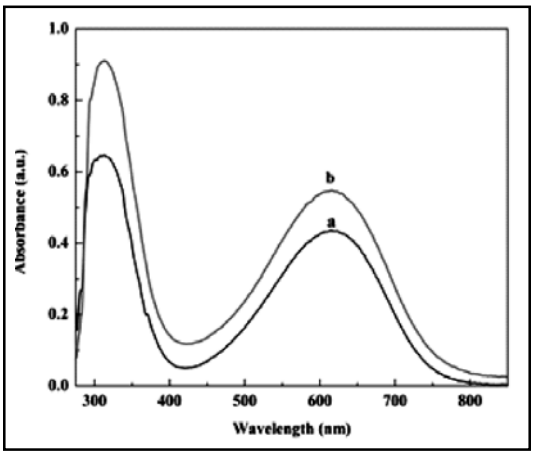

Fig. 3. UV-vis spectra of (a) POT and (b) PTC.

Furthermore, the wavelength blue shifted is also due to the interaction between oxygen in TiO_2 and –NH in POT, which thus affect the regularity and conjugated degree of POT. This result is consistent with FT-IR spectra of PTC.

3.3. XRD analysis

Figure 4 shows the XRD patterns of TiO_2, POT and PTC. It can be seen that the XRD patterns of POT show a broad amorphous diffraction band at 2θ=25°, which is the characteristic diffraction band of POT. This band may be assigned to the scattering from POT chains at interplanar spacing [22]. Fig. 4c shows the XRD patterns of PTC exhibiting the diffraction bands of both POT and TiO_2, which confirms the presence of both components in PTC. However, the intensity of diffraction bands for PTC is lower than that of pure POT and TiO_2, indicating that POT deposited on the surface of TiO_2 nanoparticle has no effect on the crystalline structure of TiO_2, the presence of noncrystalline POT reduces the mass-volume percentage of TiO_2 and sequentially weakens diffraction bands of TiO_2 [23].

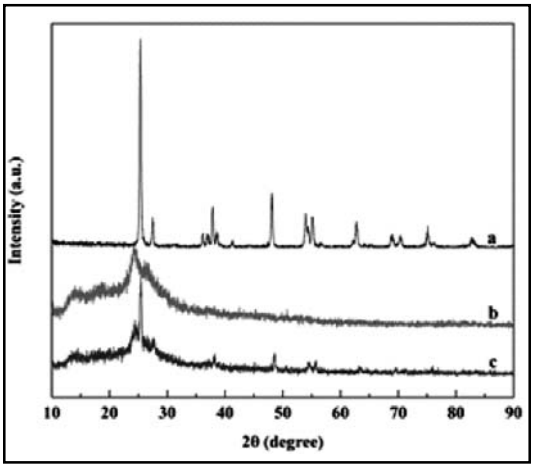

Fig. 4. XRD patterns of (a) TiO_2, (b) POT and (c) PTC.

3.4. SEM analysis

Figure 5 shows the SEM images of TiO_2, POT and PTC. From Fig. 5b, it can be seen that

POT exhibited a sponge like structure formed into irregular agglomerations, which connected with each other and the structure existed some pores. When TiO_2 nanoparticles dispersed in the reaction system, it acted as the reaction cores, resulting in the deposition of OT monomer on the surface of TiO_2 nanoparticles and in subsequent the formation of POT. It can

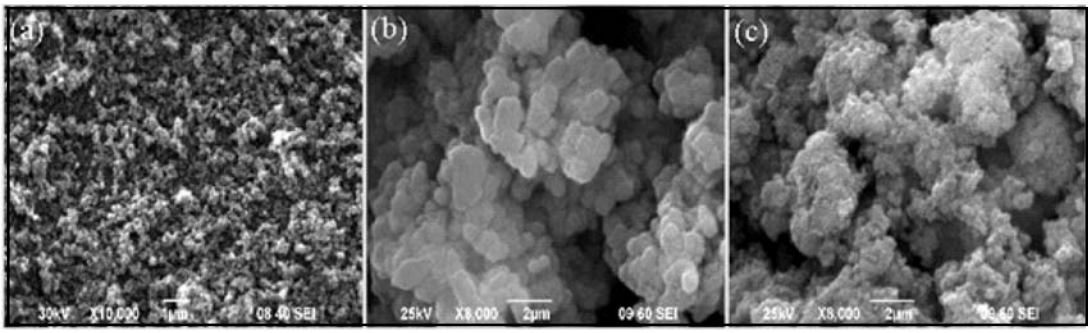

Fig. 5. SEM images of (a) TiO_2, (b) POT and (c) PTC.

be seen from Fig. 5c that the crystalline TiO_2 nanoparticles fully covered by POT formed into PTC. It indicates that TiO_2 nanoparticles were encapsulated into POT matrix structure which could significantly improve the densification structure.

3.5. TGA analysis

Figure 6 shows the TGA curves of POT and PTC. As can be seen from Fig. 6, the thermal behaviors of two materials are similar and both exhibit a two stage weight loss process. The first stage weight loss of POT is from 25 °C to 120 °C which attributes to the expulsion of water and HCl dopant from POT matrix [24,25]. The second stage weight loss is recorded at 172 °C due to the degradation of the POT backbone [26]. From Fig. 6b, it can be seen that PTC shows similar degradation process to that of POT, the degradation rate of PTC is lower than that of POT in the two stages. In addition, the residual percentage of POT is 44.5% at 800 °C while the PTC is 56.3%. The residual percentage difference between POT and PTC is considered as the content of TiO_2 nanoparticles [27]. Therefore, it can be estimated

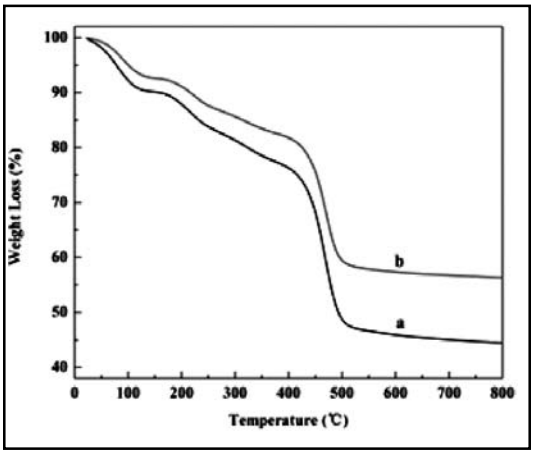

Fig. 6. TGA curves of (a) POT and (b) PTC.

that the weight ratio of POT and TiO_2 nanoparticles is about 4:1. These results indicate that the interaction between POT and TiO_2 would restrict the thermal motion of POT

in the composite and enhances the thermal stability of the composite.

3.6. Corrosion studies

The anticorrosion properties of coated steel samples were investigated in 3.5% NaCl solution as corrosion environment using potentiodynamic polarization and electrochemical impedance spectroscopy (EIS) measurements. Meanwhile, we have established the corrosion model of PTC/EP composite coated steel and also analyzed the corrosion protection mechanism.

3.6.1. Potentiodynamic polarization measurement

The potentiodynamic polarization is an important parameter to evaluate the anticorrosion properties of the coatings. Figure 7 shows the potentiodynamic polarization curves of uncoated and coated steel samples immersed in 3.5% NaCl solution for a period of time. The corrosion parameters were estimated from the intersection point of the cathode section and the anode section. The corrosion data include the corrosion potential (E_{corr}), corrosion current density (I_{corr}) and corrosion rate (*CR*) were summarized in Table 2. Generally, the higher of E_{corr}, the lower I_{corr} and *CR* indicate the better corrosion protection ability [28].

As shown in Fig. 7 and Table 2, it can be seen that the E_{corr}, I_{corr} and *CR* values of uncoated steel in 3.5% NaCl solution are found to be -846 mV, 2.45×10^{-5} A/cm^2 and 2.87×10^{-1} mm/a, respectively. When epoxy resin was coated onto the steel surface, the E_{corr} values increased to –683 mV and the I_{corr} values decreased to 2.19×10^{-6} A/cm^2, and the *CR* values decreased as a result of the reduction in I_{corr} values, which is approximately 11 times lower than that of uncoated steel. When the steel surface was coated with POT/EP composite coating, the E_{corr} values increased to –560 mV, while the I_{corr} values decreased to 3.98×10^{-7} A/cm^2 and the *CR* values decreased to 4.65×10^{-3} mm/a. These results may result from the electrochemical protection mechanism of POT, which was mainly contribute to the formation of Fe_3O_4 and γ-Fe_2O_3 as precursors of a passive layer to protect the underlying steel [29]. The larger molecular size of POT dispersed in epoxy coating also facilitates the stronger adhesive strength on the steel surface and decreases the effective area of corrosion reaction by blocking the reaction sites [30]. The E_{corr}, I_{corr} and *CR* values of PTC/EP composite coated steel in 3.5% NaCl solution were found to be -459 mV, 1.02×10^{-7} A/cm^2 and 1.19×10^{-3} mm/a, respectively. Compared to POT/EP composite coated steel, the E_{corr} values increase by about 101 mV and the I_{corr} values decrease by about 2.96×10^{-7} A/cm^2, and lower the *CR* values of the steel by approximately 4 times. These results indicate that PTC/EP composite coating exhibited a better corrosion protect on the steel surface. Generally, the corrosion protection efficiency (*PE*%) was also used to judge the anticorrosion properties of the coatings, which was calculated using the equation [31]:

$$PE\% = \frac{R_{p(coated)} - R_{p(uncoated)}}{R_{p(coated)}} \times 100\%$$

Where the polarization resistance (R_p) values were calculated from potentiodynamic polarization curves, according to the Stearn-Geary equation [32]:

$$R_P = \frac{b_a b_c}{2.303(b_a + b_c) I_{corr}}$$

The I_{corr} valves were determined by an intersection of the linear portions of the anodic and cathodic sections of the potentiodynamic polarization curves, and b_a and b_c ($\Delta E/\Delta logI$) were anodic and cathodic Tafel slopes. From the above equations, it can be calculated from the potentiodynamic polarization data that the *PE%* of pure EP coated steel, POT/EP composite coated steel and PTC/EP composite coated steel were about 71.96, 92.63 and 97.85%. These results reveal that PTC composite containing coating effectively protects the steel substrate and reduces the porosity of the composite coatings. The porosity (*P*) of the coatings was calculated using the following formula [33]:

$$P = \frac{R_{p(uncoated)}}{R_{p(coated)}} 10^{-\left(\frac{|\Delta E_{corr}|}{b_a}\right)}$$

The ΔE_{corr} was the difference values between the corrosion potentials and b_a was the anodic Tafel slope of the uncoated steel sample. From the above formula, the porosity of pure EP coated steel, POT/EP composite coated steel and PTC/EP composite coated steel were found to be about 4.29, 0.27 and 0.025%. It suggests that the porosity would decrease with the presence of TiO_2 nanoparticles and POT. Undoubtedly, the corrosion protection efficiency and porosity of the coatings indicate that PTC/EP composite coating provides better barrier properties for blocking the electrolyte access to the steel surface. All results demonstrates that the enhanced corrosion protection of PTC/EP composite coated steel was a result of PTC

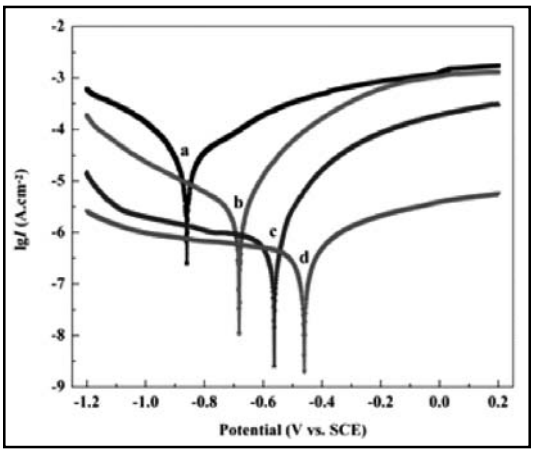

Fig. 7. Potentiodynamic polarization curves of (a) uncoated steel, (b) pure EP coated steel, (c) POT/EP coated steel and (d) PTC/EP coated steel in 3.5% NaCl solution.

TABLE 2. The corrosion data of uncoated and coated steel samples in 3.5% NaCl solution by potentiodynamic polarization measurement.

Samples	E_{corr} (mV)	I_{corr} (A/cm^2)	*CR* (mm/a)	R_p (kΩ.cm^2)	*PE* (%)	*P* (%)
Uncoated steel	-846	$2.45´10^{-5}$	2.87×10^{-1}	2.96	/	/
Pure EP coated steel	-683	2.19×10^{-6}	2.56×10^{-2}	10.56	71.96	4.29
POT/EP coated steel	-560	3.98×10^{-7}	4.65×10^{-3}	40.18	92.63	0.27
PTC/EP coated steel	-459	1.02×10^{-7}	1.19×10^{-3}	138.37	97.85	0.025

fillers dispersed in epoxy coating both improve the barrier and passivation effects. PTC/EP composite coating containing three type materials and enjoying the combined properties acts as a fence structure that block the diffusion of corrosion substances.

3.6.2. EIS measurement

The EIS was also an important parameter to judge the anticorrosion properties of the coatings. Generally, in order to accurately analyze the impedance data and understand the anticorrosion mechanism of the coating films, the simple equivalent circuit model (Randles equivalent circuit) was proposed in Figure 8. The model included a charge transfer resistance in paralleled with a double layer capacitance and in series with a solution resistance. Furthermore, the impedance (Z) depended on the solution resistance (R_s), charge transfer resistance (R_{ct}), double layer capacitance (C_{dl}) and the frequency of the AC signal (ω). It can be explained by the following equation [34]:

$$Z = Z' + jZ'' = R_s + \frac{R_{ct}}{1+(R_{ct}C_{dl}\omega)^2} + j\frac{R_{ct}^2 C_{dl}\omega}{1+(R_{ct}C_{dl}\omega)^2}$$

Where the high frequency intercept corresponds to the R_s, and the low frequency intercept corresponds to the sum of the R_s and R_{ct} [35,36]. The R_{ct} was calculated as the difference between the high and low frequency intercepts. Obviously, a larger diameter of the semicircle loop (charge transfer resistance) indicates a lower corrosion rate[37].

Figure 9 shows the EIS curves of uncoated and coated steel samples immersed after few days in 3.5% NaCl solution. It can be observed from Fig. 9 that the EIS curves of all steel samples show similar characteristics, the diameter of EIS curves (a-d) reveal that the diameter of PTC/EP composite coated steel is the highest and the uncoated steel is the lowest. From Fig. 9, the R_{ct} valves of uncoated steel, pure epoxy coated steel, POT/EP composite coated steel and PTC/EP composite coated steel were calculated to be about 0.80, 3.52, 7.09 and 9.72 kΩ.cm^2. It is further noted that the charge transfer resistance of PTC containing coating is significantly higher than that of POT and pure EP, which means PTC/EP composite coating provides an excellent corrosion inhibition to steel substrate. This result is in accordance with potentiodynamic polarization measurement. The increased resistance values of PTC containing coating may be due to its relative good dispersity so that it

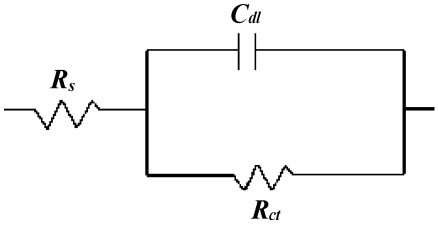

Fig. 8. The equivalent circuit model of uncoated and coated steel samples for EIS measurements.

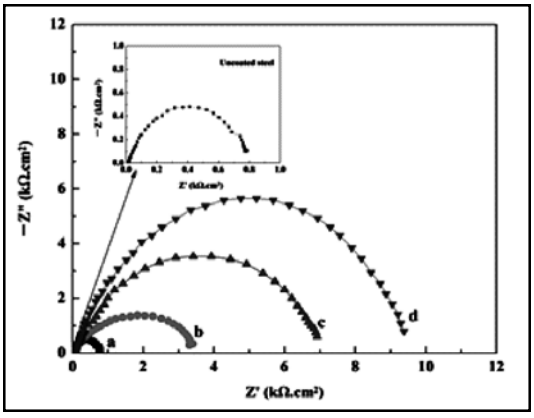

Fig. 9. EIS curves of (a) uncoated steel, (b) pure EP coated steel, (c) POT/EP coated steel and (d) PTC/EP coated steel in 3.5% NaCl solution.

can be distributed uniformly in epoxy coating, which can facilitate to maintain the uniformly passive layer on the steel surface. In addition, this is also due to the barrier effects of TiO_2 nanoparticles, which can more effectively increase the tortuosity of the diffusion pathway of oxygen, water and chloride ions.

Figure 10 shows the corrosion schematic diagram of PTC/EP composite coated steel immersed in 3.5% NaCl solution. It is conceived that PTC/EP composite coating protects the underlying steel from corrosion, which at least exists two protect mechanisms as follow [38,39]: 1) Physical barrier effect. The coating works as a barrier coating against the diffusion of the

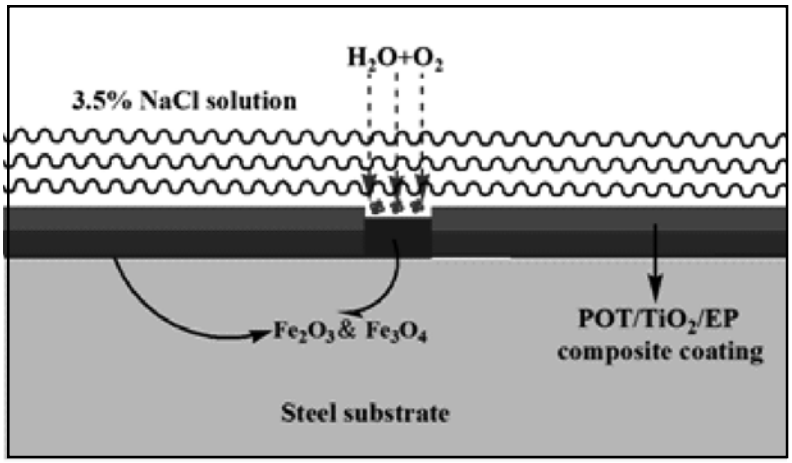

Fig. 10. The corrosion schematic diagram of PTC/EP composite coated steel in 3.5% NaCl solution.

electrolyte and corrosion ions. 2) Passivation effect. Under immersion conditions, the presence of POT in the composite coating maintains the passive state on the steel substrate by the oxidation reduction reaction of the POT. It can be understand that the conceivement is in correspond with the above electrochemical corrosion analysis.

From the above corrosion schematic diagram, it can be seen that corrosion processes need sufficient water and oxygen for the formation of rust and dissolution of the steel. If any of these processes are prevented, the corrosion is inhibited and the coating becomes effective for corrosion protection. So it is reasonable to believe that increasing the tortuosity of the diffusion pathways is able to effectively prevent the water and oxygen from accessing the steel substrate, leading to a good corrosion protective effect. Sum up the analysis results of potentiodynamic polarization and EIS measurement, the PTC/EP composite coating shows an effective protection to the steel substrate because of its good barrier effects. The composite coating containing both POT and TiO_2 nanoparticles can lead to much better anticorrosion properties than that of the single component systems.

4. CONCLUSIONS

Poly(o-toluidine)/nano TiO_2 composite was prepared by in situ polymerization method. FT-IR and UV-vis spectra indicated that the interactions between POT chains and TiO_2 nanoparticles would lead to the shift of the characteristic absorption peaks of POT. XRD patterns confirmed that PTC exhibited the diffraction peaks of both POT and TiO_2 nanoparticles, and the crystalline performance of TiO_2 nanoparticles is not affected by POT. SEM images suggested that TiO_2 nanoparticles were fully covered by POT matrix, and significantly improved the compact structure of POT molecules. TGA curves indicated that TiO_2 nanoparticles could improve the thermal properties of the composite and drop the degradation rate of the composite. The potentiodynamic polarization of all coated steel samples in 3.5% NaCl solution have shown that PTC/EP composite coating was applied on steel substrate with 97.85% protection efficiency. EIS measurement also showed that the PTC/EP composite coating exhibited a higher charge transfer resistance and it provided an excellent corrosion inhibition to steel substrate. The higher corrosion protection properties of PTC fillers containing coating was associated with the formation of more uniformly passive layer on the steel surface, and the addition of TiO_2 nanoparticles which act as a fence structure that increased the tortuosity of the diffusion pathway of corrosive substances.

Acknowledgments

The authors are grateful for the financial support of the National Natural Science Foundation of China (Nos. 51274057, 51474057) and Initial Scientific Research Fund of Young Teachers (No.N140203003), and also thankful to Northeastern University providing the facilities for the research.

REFERENCES

1. E. Hür, G. Bereket and Y. ª ahin, *Curr. Appl. Phys.* **7** (2007) 597.
2. Z. T. Li, L. Ma, M. Y. Gan, J. Yan, H. F. Hu, J. Zeng, and F. F. Chen, *Polym. Compos.* **34** (2013) 740.
3. J. Yan, Y. W. Yang, L. Ma, M.Y. Gan and X. Li, *Polym. Compos.* **36** (2015) 1541.
4. K. F. Khaled and N. Hackerman, *Electrochim. Acta.* **48** (2003) 2715.
5. P. Savitha and D. N. Sathyanarayana, *Synth. Met.* **145** (2004) 113.
6. P. Savitha and D. N. Sathyanarayana, *Polym. Int.* **53** (2004) 106.
7. S. Sathiyanarayana, S. K. Dhawan, D. C. Trivedi and K. Balakrishnan, *Corros. Sci.* **33** (1992) 1831.
8. A. P. Srikanth, V. Raman, S. Tamilselvi, S. Nanjundan and N. Rajendran, *Anti-Corros. Methods Mater.* **55** (2008) 3.
9. S. Sathiyanarayana, and K. Balakrishnan, *Electrochim. Acta.* **39** (1994) 831.
10. L. Ma, C. Q. Huang and M. Y. Gan, *J. Appl. Polym. Sci.* **127** (2013) 3699.
11. B. K. Sharma, A. K. Gupta, N. Khare, S. K. Dhawan and H. C. Gupta, *Synth. Met.* **159** (2009) 391.
12. V. Eskizeybek, F. Sarı, H. Gülce, A. Gülce and A. Avcı, *Appl. Catal. B: Environ.* **119** (2012) 197.
13. V. H. Nguyen, L. L. Tang and J. J. Shim, *Colloid. Polym. Sci.* **291** (2013) 2237.
14. A. Mostafaei and F. Nasirpouri, *Prog. Org. Coat.* **77** (2014) 146.
15. R. C. Rathod, S. S. Umare, V. K. Didolkar, B. H. Shambharkar and A. P. T. Patil, *Indian. I. Metals.* **66** (2013) 97.

16. S. X. Min, F. Wang and Y. Q. Han, *J. Mater. Sci.* **42** (2007) 9966.

17. K. Mallick, M. J. Witcomb and M. S. Scurrel, *Eur. Polym. J.* **42** (2006) 670.

18. Y. J. He, *Chem. Phys.* **92** (2005) 134.

19. J. C. Xu, M. Liu and H. L. Li, *Mat. Sci. Eng. C.* **25** (2005) 444.

20. A. Pron and P. Rannou, *Prog. Polym. Sci.* **27** (2002) 135.

21. M. V. Kulkarni and A. K. Viswanath, *Eur. Polym. J.* **40** (2004) 379.

22. S. X. Wang, Z. C. Tan, Y. S. Li, L. X. Sun and Y. Li, *Thermochim. Acta.* **441** (2006) 191.

23. S. G. Pawar, S. L. Patil, M. A. Chougule, A. T. Mane, D. M. Jundale and V. B. Patil, *Int. J. Polym. Mater.* **59** (2010) 777.

24. S. X. Wang, L. X. Sun, Z. C. Tan, F. Xu and Y. S. Li, *J. Therm. Anal. Calorim.* **89** (2007) 609.

25. M. Çelik and M. Önal, *J. Polym. Res.* **14** (2007) 313.

26. Y. N. Qi, F. Xu, H. J. Ma, L. X. Sun, J. Zhang and T. Jiang, *J. Therm. Anal. Calorim.* **91** (2008) 219.

27. J. Zhang, D. Shu, T. R. Zhang, H. Y. Chen, H. M. Zhao, Y. S. Wang, Z. J. Sun, S. Q. Tang, X. M. Fang and X. F. Cao, *J. Alloys Compd.* **532** (2012) 1.

28. C. H. Chang, T. C. Huang, C. W. Peng, T. C. Yeh, H. I. Lu, W. I. Hung, C. J. Weng, T. I. Yang and J. M. Yeh, *Carbon* **50** (2012) 5044.

29. B. Wessling, *Synth. Met.* **85** (1997) 1313.

30. A. Benchikh, R. Aitout, L. Makhloufi, L. Benhaddad and B. Saidani, *Desalination.* **249** (2009) 466.

31. P. Pawar, A. B. Gaikwad and P. P. Patil, *Electrochim. Acta.* **52** (2007) 5958.

32. A. H. Navarchian, M. Joulazadeh and F. Karimi, *Prog. Org. Coat.* **77** (2014) 347.

33. S. Chaudhari, A. B. Gaikwad and P. P. Patil, *J. Coat. Technol. Res.* **7** (2010) 119.

34. K. C. Chang, W. F. Ji, M. C. Lai, Y. R. Hsiao, C. H. Hsu, T. L. Chuang, Y. Wei, J. M. Yeh and W. R. Liu, *Polym. Chem.* **5** (2014) 1049.

35. C. M. Goulart, A. E. Souza, C. A. M. Huitle, C. J. F. Rodrigues, M. A. M. Maciel and A. Echevarriaa, *Corros. Sci.* **67** (2013) 281.

36. K. S. Jacob and G. Parameswaran, *Corros. Sci.* **52** (2010) 224.

37. K. F. Khaled, Mater. *Chem. Phys.* **112** (2008) 290.

38. S. Sathiyanarayanan, S. S. Azim and G. Venkatachari, *Synth. Met.* **157** (2007) 205.

39. S. Sathiyanarayanan, S. S. Azim and G. Venkatachari, *Prog. Org. Coat.* **59** (2007) 291.

Received: 16-05-2016

Accepted: 25-12-2017